Volumetric Correlation PIV: a New Technique for 3D Velocity Vector Field Measurement

Andreas Fouras[1,2,3], David Lo Jacono[2,4], Chuong V. Nguyen[2,5], Stephen Dubsky[1,2,6], Kerry Hourigan[1,2,7]

1: Department of Biological Engineering, Monash University, Melbourne, Australia
2: Fluids Laboratory for Aeronautical and Industrial Research (FLAIR), Monash University, Melbourne, Australia
3: Fouras@eng.monash.edu, 4: David.LoJacono@eng.monash.edu.au, 5: Chuong.Nguyen@eng.monash.edu.au
6: Stephen.Dubsky@eng.monash.edu.au, 7: Kerry.Hourigan@eng.monash.edu.au

Abstract: A method is proposed that allows three-dimensional (3D) two-component measurements to be made by means of particle image velocimetry (PIV) in any volume illuminated over a finite thickness. The method is based on decomposing the cross-correlation function into various contributions at different depths. Because the technique is based on 3D decomposition of the correlation function and not reconstruction of particle images, there is no limit to particle seeding density as experienced by 3D particle tracking algorithms such as defocusing PIV and tomographic PIV. Correlations from different depths are differentiated by the variation in point spread function of the lens used to image the measurement volume over that range of depths. A number of examples are demonstrated by use of synthetic images which simulate micro-PIV (µPIV) experiments. These examples vary from the trivial case of Couette flow (linear variation of one velocity component over depth) to a general case where both velocity components vary by different complex functions over the depth. The method could also be used with thick light sheets in macro-scale PIV and in a stereo configuration for 3D three-component PIV.

1. Background

Since its general acceptance as a powerful measurement tool for fluid mechanics, researchers have been searching for means of increasing the dimensionality of PIV above the standard two component velocity measurement over a plane. Throughout the paper the mDnC notation will be used, where m represents the dimension of the measurement volume and n represents the dimension of the resolved displacements. As an example, two component velocity measurements over a plane are expressed 2D2C measurements in this notation.

For three components of velocity vectors over a measurement plane, stereo PIV (SPIV) was one of the first variations in PIV methodology to be introduced. Since its first development (Arroyo and Greated, 1991) through to more recent advances (Fouras *et al*, 2007a, 2008), SPIV has been becoming better understood, more accurate and simpler to implement. With 2D3C systems, six of the nine terms of the velocity gradient tensor are available. In order to obtain all nine terms of the velocity gradient tensor, a pseudo 3D3C system is available by conducting SPIV on two adjacent planes. Multi-plane SPIV (Schroder and Kompenhans, 2004; Kahler, 2004) allows for differentiation across planes to obtain those additional three spatial velocity gradients.

Holographic PIV (HPIV) (Barnhart *et al*, 1994; Zhang *et al*, 1997) allows for truly 3D3C velocity measurements. This broad range of techniques has, in its various forms, advantages and disadvantages. In-line HPIV, and more recently available Digital In-line HPIV, is perhaps the simplest and easiest to implement, but is limited by signal to noise ratio (SNR). Furthermore, there is a limit to the total number of particles that can be resolved and therefore a limited number of vectors are achievable. Off-axis HPIV, which does not have this limitation, is dramatically more complex to implement and requires considerable greater laser power. Although HPIV has

demonstrated ability to accurately resolve 3D3C velocity fields, due to complexity and expense of implementation, HPIV has not enjoyed wide popularity.
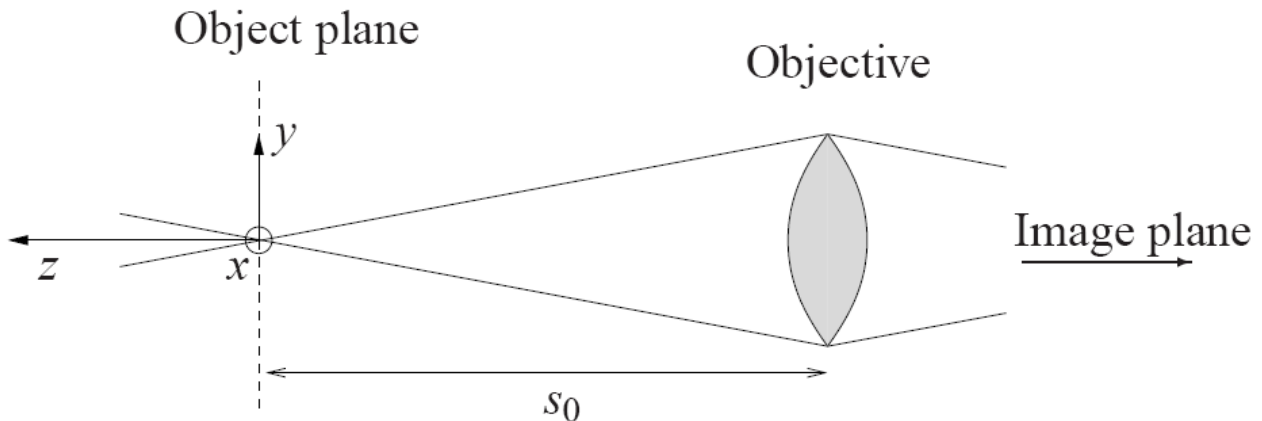

Fig. 1 Schematic diagram of generic apparatus including coordinate system. The object plane (also the focal plane) is at the distance s_0 from the objective. The origin of the coordinates is the center of the object plane.

A different approach to that of Holography is Tomographic image reconstruction. Tomographic PIV (Elsinga *et al*, 2006) utilises multiple cameras in different positions to image an illuminated volume. A 3D image pair is reconstructed and 3D cross-correlation analysis is performed. This technique, although recent, shows promise as an alternative 3D3C measurement tool. Unfortunately, like other techniques that reconstruct the image rather than the velocity field, this approach is also limited by the number of particles that can be resolved.

A simpler to implement, elegant technique that achieves 3D3C results is defocusing PIV (Willert and Gharib, 1992; Pereira *et al*, 2000). This technique utilises a lens mask to alter the point spread function (PSF) of the imaging system. The mask creates a PSF that is asymmetric about the focal plane. Particles out of focus appear as triangles, which invert as they cross the focal plane. Despite the elegance and utility of this technique, it is poorly named – this technique allows particles to be tracked throughout the illuminated volume, producing 3D3C particle tracking velocimetry (PTV). PTV is clearly distinguishable from PIV both by seeding density levels and the use of correlation functions for measurement of displacement. As a PTV variant, this technique is necessarily limited in the number of particles that can be individually identified. Furthermore, the introduction of the lens mask substantially reduces the light gathering power of the imaging system. Despite these limitations, the technique is gaining popularity and has achieved some considerable success recently (Forouhar *et al*, 2006). Another development similar to defocusing PIV is based on deconvolution imaging (Park and Kihm, 2006). This once again allows the direct identification and measurement of particles in 3D space allowing 3D3C PTV.

As discussed, many techniques are available that have successfully resolved 3D3C vector fields. However, these techniques are typically based on the reconstruction of particle images, followed by either 3D cross-correlation or particle tracking analysis, which limits maximum spatial resolution. Furthermore, these techniques require additional or modified hardware not required for traditional PIV. This paper proposes a novel approach to gaining three-dimensional velocity vector fields without this spatial resolution limitation. The key principle is to conduct further analysis of the calculated correlation function, of single camera PIV images, to obtain the three-dimensional information. This results in a system that is identical to traditional PIV implementations, differing only in the analysis of images post-acquisition. The technique is based on 3D decomposition of the correlation function into various contributions at different depths.
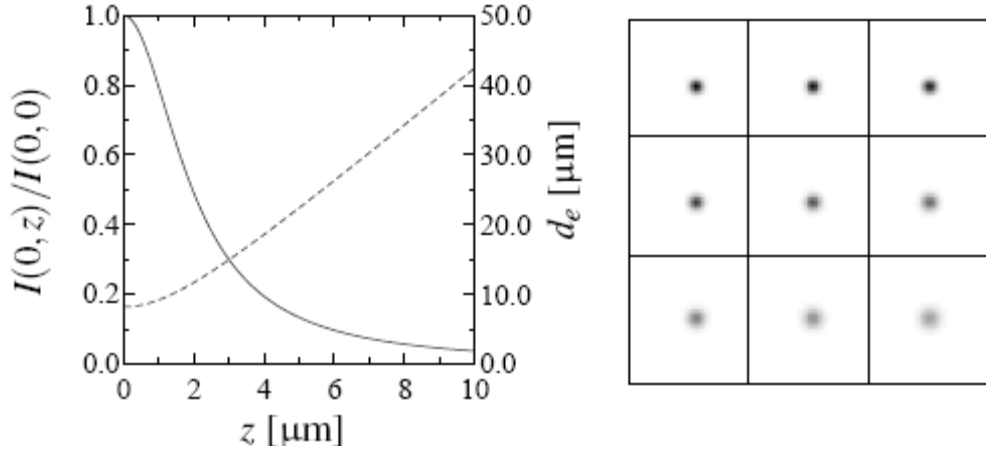
Fig. 2 (a) Normalised particle image intensity, and effective diameter as a function of depth, distance from focal plane z, following Eqs. (1) and (2), represented by the solid and dashed line, respectively (Olsen and Adrian, 2000b). (b) Example of particle images at nine different depths from the focal plane, with depth increasing from left to right, top to bottom.

2. Introduction

It is well understood that particle images appear differently when they are not on the focal plane. Olsen and Adrian (2000b) discuss the effect of these out-of-focus particles on the measurement of the velocity field. In micro-PIV (µPIV) systems, the entire volume is illuminated. Therefore several aspects of an out-of-focus particle contribute to the velocity measurements, such as the variation in particle image intensity and diameter as a function of distance from the focal plane. A schematic diagram of the optical and geometrical parameters, including coordinate system, is shown in Fig. 1.

For a given particle diameter d_p and a given set of magnification M, focal number $f^{\#}$ and lens aperture diameter D_a, Olsen and Adrian (2000b) derived the expression of the effective diameter and the intensity distribution of that given particle as a function of depth as seen in the image plane:

$$d_e(z)^2 = M^2 d_p^2 + 5.95(M+1)^2 \lambda^2 f^{\#2} + \frac{M^2 z^2 D_a^2}{(s_0+z)^2}, \tag{1}$$

$$I(r,z) = I_0 \exp\left(\frac{-4\beta^2 r^2}{d_e^2}\right), \tag{2}$$

with

$$I_0 = \frac{J_p D_a \beta^2}{4\pi d_e^2 (s_0+z)^2}, \tag{3}$$

where λ is the wavelength of the laser, J_p the flux of light emitted from the particle and $\beta^2 = 3.67$ (Adrian and Yao, 1985). The key assumptions are uniform particle diameter and laser intensity, isotropic light emission and that both the geometric optics term and the diffraction term can be approximated as Gaussian. To illustrate this, Eqs. (1) and (2) are represented in Fig. 2a, for $M = 5$, $f^{\#} = 1$, $d_p = 0.5 \mu m$, and $D_a = 9000 \mu m$. The effect of out-of-focus particles is shown also in Fig. 2b. Figure 2b shows the increase of the effective particle diameter and decrease of the peak light intensity emitted as the distance between the particle and the object plane (or focal plane) increases.

Of interest, Meinhart *et al* (2000a) and Olsen and Adrian (2000b) introduced the depth of correlation parameter. It defines the depth over which particles significantly contribute to the

correlation function $2z_{corr}$ for "simple flowfields". This relation must be modified if the flowfield contains either significant Brownian motion (Olsen and Adrian, 2000a) or out-of-plane motion (Olsen and Bourdon, 2003). Here, z_{corr} is given by:

$$z_{corr} = \left[\frac{1-\sqrt{\varepsilon}}{\sqrt{\varepsilon}} \left(f^{\#} d_p (z)^2 + \frac{5.95(M+1)^2 \lambda^2 f^{\#4}}{M^2} \right) \right]^2, \tag{4}$$

where ε is the ratio of the correlation contribution of a particle of $z = 0$ to the correlation contribution at z. Typically, the choice $\varepsilon = 0.01$ is reasonable (Olsen and Adrian, 2000b). It is important to note that for cases where the PSF does not match aforementioned Eq. (1) and Eq. (2), it has been shown (Bourdon *et al*, 2004) that the PSF can be readily measured experimentally.

It had previously been thought (Meinhart *et al*, 2000a; Olsen and Adrian, 2000b) that the major problem in μPIV is that the out-of-focus particles in as far as they contribute to the correlations produce bias. Therefore, several attempts have been made to overcome these difficulties by filtering, subtracting, and then tracking these particles. It is proposed here that the additional information provided by these out-of-focus particles should not be discarded. Instead, it provides the opportunity to resolve the displacement as a function of depth.

3. Description of New Technique

The technique described in this paper is derived from an X-ray PIV method capable of measuring 3D2C velocity fields under certain flow conditions (Fouras *et al*, 2007b). The differences in approach and results are a direct consequence in the differences between imaging modalities. In the X-ray imaging system described in Fouras *et al* (2007b), the effective depth of focus is infinite and hence no depth information is recorded.

This proposed technique is based on the proposition that at any (x, y) location, the full cross-correlation function C_{full} of the image pairs at that location is equal to the sum of cross-correlation functions at each depth, C_{2D}, each with its own δ_x, δ_y and PSF. This can be expressed as:

$$C_{2D}(\hat{x}, \hat{y}, z) = \alpha I_0(z) \exp\left(-\frac{\|\hat{x} - \delta\|^2}{2\sigma(z)} \right) \tag{5}$$

$$C_{full}(\hat{x}, \hat{y}) = \alpha \sum_{z=z_{min}}^{z_{max}} C_{2D}(\hat{x}, \hat{y}, z), \tag{6}$$

where $\sigma = Md_e$ is the effective particle diameter in the image plane measured in pixels, and z_{min} and z_{max} are the boundaries of the illuminated particle field.

To further assist in the description of the technique, the Couette flow is considered; that is, a uniform shear through a channel of depth *h*. Synthetic image pairs of particles (separated by a given δt) within the whole channel have been generated, using Eqs. (1) and (2). The synthetic image pairs are then cross-correlated to yield the cross-correlation function.
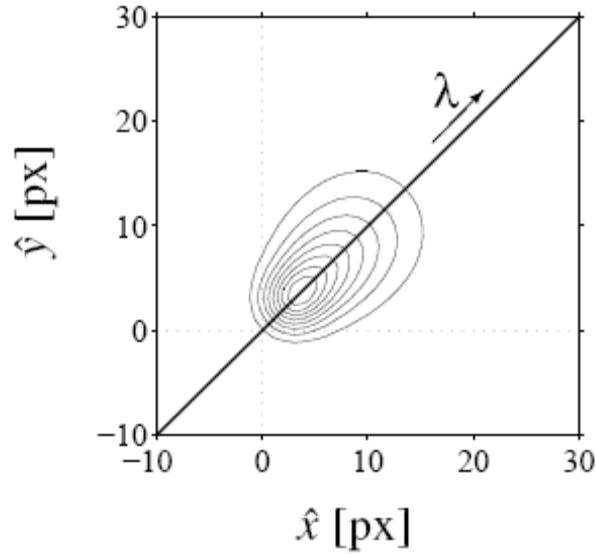
Fig. 3 An averaged cross-correlation function for a Couette flow. The curvilinear coordinate λ represents the relationship between $\hat{x}$ and $\hat{y}$ – the direction of the flow. Note that for this flow λ lies on the maximum envelope of the cross-correlation peak.

Figure 3 shows the measured cross-correlation function, C_{meas}, obtained for this flow viewed at a $45°$ angle. The coordinates in the cross-correlation space are $\hat{x}$ and $\hat{y}$. It can be seen that the pattern is not representative of a Gaussian distribution, as one would expect from cross-correlation of focused particles, but is stretched along λ, the direction of the flow. Therefore, the pattern populates *all* the velocities occurring in the illuminated field. It is clear that if one were to take the maximum of the peak – as is done in classical PIV – the displacement obtained would be a complex
function of both the velocity profile and the PSF. This justifies previous attempts of narrowing the depth of field in order to minimise this bias.

In the case of Couette flow, or any other unidirectional flow, the λ coordinate can be trivially expressed with $(\hat{x}, \hat{y})$. The aim as stated earlier in the section is to find a $\underline{\delta}(z)$ such that $C_{full}(\hat{x}, \hat{y})$ approaches $C_{meas}(\hat{x}, \hat{y})$. This approach is only valid while I_0 and d_e are unique for all z in the measurement volume. As Eqs. (1) and (2) are symmetric about the focal plane, this uniqueness is achieved by placing the focal plane outside the measurement volume. The ideal case is to utilise the linear region of the $I_0(z)$ and $d_e(z)$ functions. However the maximum intensities of particles far from the focal plane also need to be considered in combination with the bit depth of the acquisition system.

This solution is implemented via a non-linear least squares solver. To achieve this, it is most convenient to express the solution $\delta_x(z)$ and $\delta_y(z)$ as continuous analytical functions. The choice of these functions is arbitrary but selected here are the piece-wise linear and cubic spline functions.

4. Results and Discussion

The technique described in this paper has been rigorously validated by the use of synthetically generated image data sets.
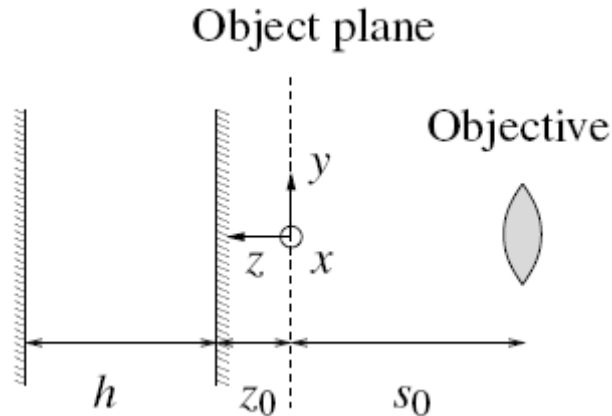
Fig. 4 Schematic diagram of the channel (depth *h*) including coordinate system. The object plane (also the focal plane) is at the distance s_0 from the objective, and at distance z_0 from the channel. The origin of the coordinates is the center of the object plane. The principal flow direction is out of the page.

4.1 Validation by synthetic data sets

A uniform channel geometry, depth $h = 6\mu m$, has been used to validate this technique. Four different flow profiles have been selected, namely a Couette flow (linear in z); Poiseuille flow (parabolic in z); separated channel flow (cubic in z); mixing-layer flow profile (tanh in z). Finally, a generalisation of the technique is proposed via a skewed (general) boundary layer profile.

For the sake of simplicity of explanation, these four seminal cases have been implemented with $\delta_y = 0$. In cases such as these, where λ is a straight line (δ_x and δ_y are linearly related), the solution is independent of the orientation of λ. In this circumstance, λ lies on the maximum envelope of the cross-correlation function and hence is easily found.

Figure 4 shows a schematic of the geometrical configuration used as well as the coordinate system. Synthetic image pairs have been generated for particles of diameter $d_p = 0.5\mu m$, magnification $M = 5$, focal number $f^\# = 1$ and aperture diameter $D_a = 9000\mu m$, typical of a µPIV setup. Similar results have been obtained for other µPIV optical configurations. The particles were located over the entire channel depth. As discussed earlier, to achieve optimal conditions for linearity without exceeding depth of correlation, a measurement volume spanning from $z_0 = 2\mu m$ to $8\mu m$ was chosen. These pairs were successively cross-correlated then averaged and normalised. As pointed out by Meinhart *et al* (2000b), averaging the cross-correlation samples overcomes problems such as insufficient seeding density and poor signal to noise ratio. Unless otherwise specified, the number samples used for each average in this study is 1024.

Figure 5 shows the results of the analysis for the test cases described above. It can be seen that in all cases the solution has successfully captured the flow over the entire depth. Furthermore, these calculated velocities are obtained with a zero initial guess. While not necessary, the computational time and accuracy are improved if the practitioner has *a priori* knowledge of the flow. However in the case where such knowledge is not available, and for complicated topologies, the spline can be supplemented with a more robust piecewise linear approach as a first step,

followed by the more refined spline implementation. An example of this approach is demonstrated in Fig 5(c) for the separated flow.

Interestingly the accuracy does not vary with the magnitude of shear, as illustrated by the increasing rates of shear from Figs. 5(a)-(d).
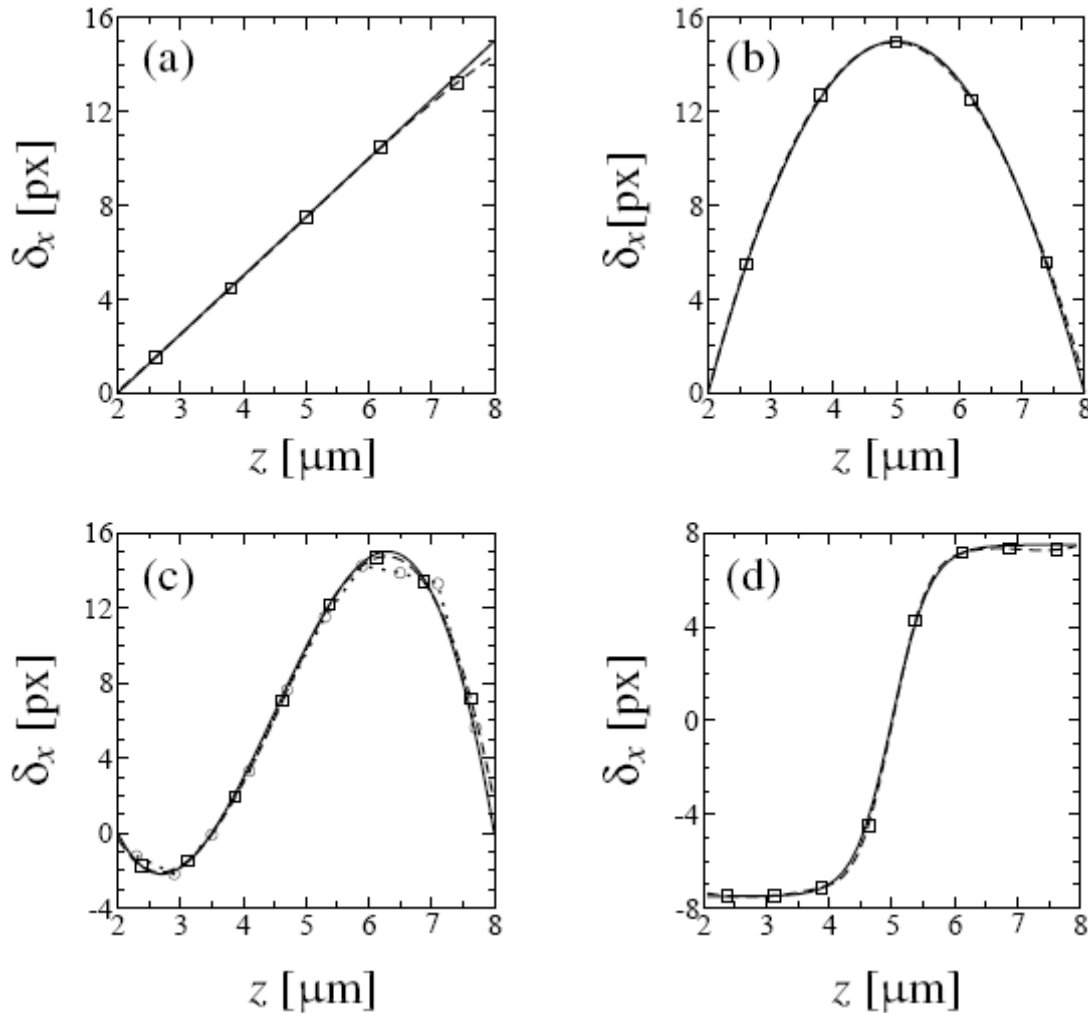

Fig. 5 Calculated values of the displacement δ_x as a function of depth for (a) Couette; (b) Poiseuille; (c) separated; (d) mixing layer. The solid line represents the exact solution. Squares represent the knots for the spline solution (dashed lines). The separated flow example illustrates the iterative approach consisting of first a linear guess (circles and dotted line) followed by a spline scheme.

Finally the authors wish to stress that all of the above examples relate to the volumetric correlation analysis of cross-correlation peaks at a single interrogation window location. These depth-resolved measurements would be available at each sampling window location throughout a PIV measurement region.

Figure 6 shows both the effect of the number of samples N of the PIV interrogation window and the effect of the particle seeding density ρ on the accuracy of the calculated solution (root mean square, RMS). Clearly, increasing the number of samples increases the accuracy of the resolved displacement field. However, even for low numbers of samples ($N=16$), the results qualitatively follow the exact solution. Furthermore, it can be seen that for low N the velocity profiles is biased towards the focal plane. The effect of seeding density follows an interesting trend, which is that

after significant benefit for increases in density at low values of density, a plateau is attained for a large range of seeding density.

To demonstrate the general applicability of this technique, we extended the analysis to different channel depths with their appropriate optical configuration. The objectives chosen are typical in µPIV as they are inexpensive and readily available.
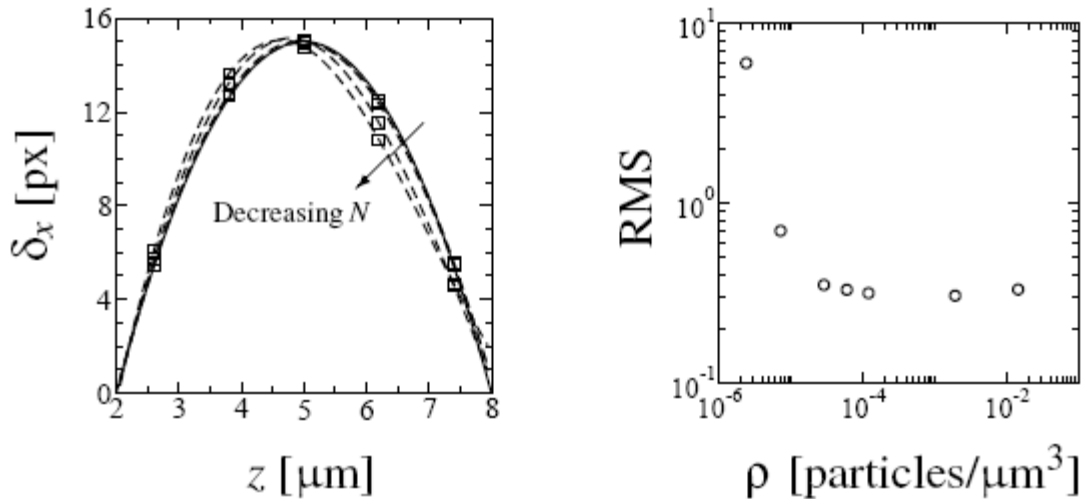
Fig. 6 Left: Effect on δ_x of the number of samples N of the PIV interrogation window; $N = 1024, 256, 64, 16$. All solutions are obtained with a 5 knotted spline (solid squares with dashed line) with a zero initial guess. Solid line represents the exact solution. Right: Effect of the particle seeding density ρ on the accuracy of the calculated solution (root mean square deviation, RMS). Data shown are for $N = 1024$.
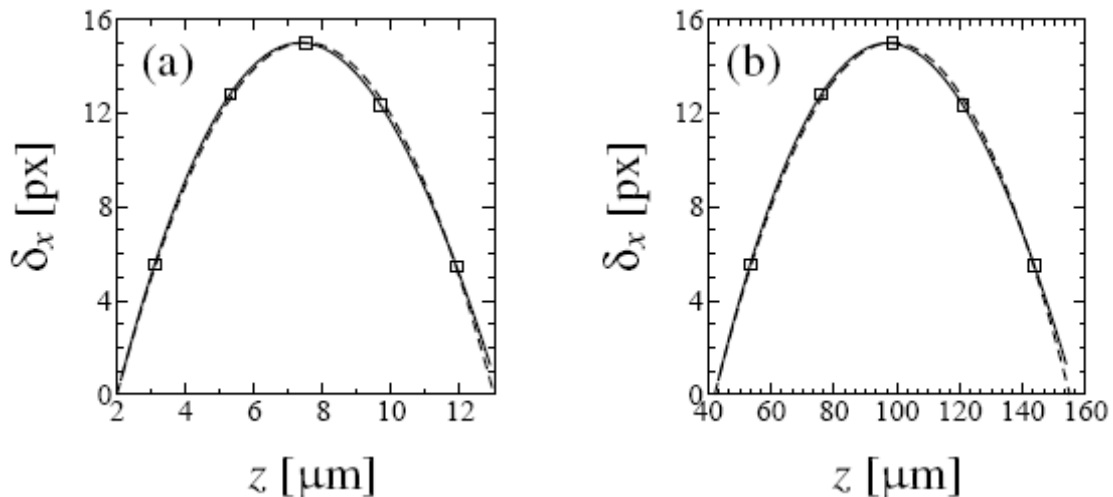
**Fig. 7** Parabolic profile for typical objectives and associated channel depth. Left: channel from 2 to 13µm with a 20×0.3 objective. Right: 42 to 155µm with 5×0.12 objective.

Figure 7 demonstrates the applicability of the technique to channels of various depths. The selected range varies from a few microns depth to over a hundred microns depth. More precisely, the notion of depth is purely arbitrary, just as is the field of view in the laser plane; in a volumetric sense the field of view is selected by the practitioner through the choice of lenses, cameras, magnification tube *etc*.

The final step of validation described in this section is the more general case where the velocity profile is skewed. In these cases δ_y cannot be expressed as a simple linear function of δ_x and λ is curved as can be seen in Fig 8. One example of flow geometries that would produce such skewed boundary layers is a channel with undulating walls (Lo Jacono *et al*, 2005).

Figure 8 shows the calculated values of the displacement field δ_x and δ_y as a function of depth for the skewed boundary layer flow. Solid lines represent exact solution. Crosses and circles represent the δ_x and δ_y components, respectively, using the piece-wise linear approach. It can be seen in this general case that the technique has worked to a high degree of accuracy, further validating the technique.
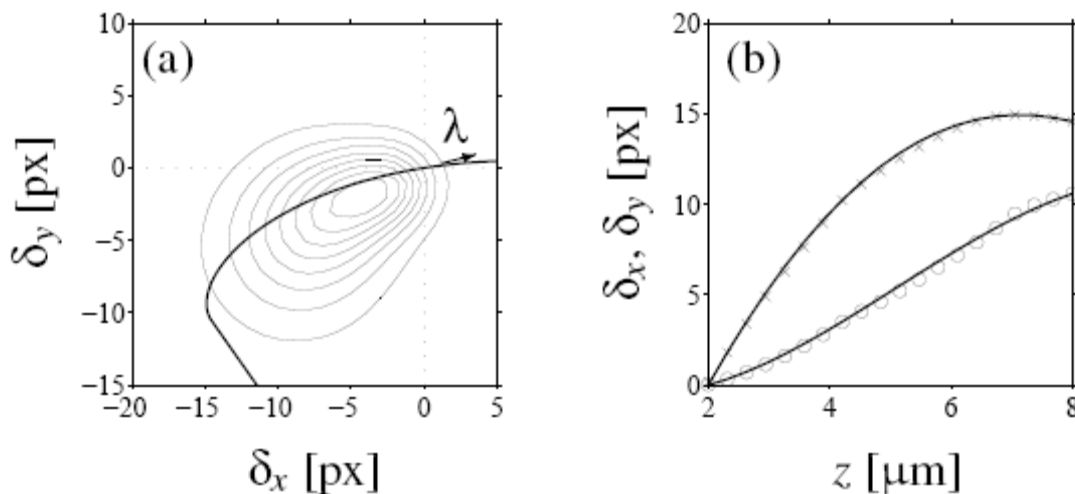
Fig. 8 (a) Average cross-correlation function for the skewed boundary layer flow. The curvilinear coordinate λ represents the relationship between δ_x and δ_y. Note that for this flow λ does not lie on the maximum envelope of the cross-correlation peak. (b) Calculated values of the displacement field δ_x and δ_y as a function of depth for the skewed boundary layer flow. Solid lines represent exact solution. Crosses and circles represent δ_x and δ_y component, respectively, using the piece-wise linear approach.

5. Conclusions

A method has been proposed that allows 3D2C measurements to be made in any volume illuminated by a light sheet of finite thickness. The method is based on the decomposition of the cross-correlation function into various contributions at different depths in the light sheet. This technique does not suffer from many of the limitations of other techniques designed to improve the dimensionality of PIV. A number of examples of the viability of this technique have been demonstrated by use of synthetic images which simulate micro-PIV experiments. These examples vary from trivial cases of linear variation of one velocity component over depth to a general case where both velocity components vary by different complex functions over depth. This technique could be implemented in both macro and micro-PIV experiments. Furthermore, this technique could be expanded by the use of a second camera and performed in stereo to yield fully 3D3C velocity vector field data with only two cameras. Alternatively in wall bounded flows, by using the continuity equation, one can recover out-of-plane velocity to achieve 3D3C measurements.

References

Adrian R, Yao C (1985) Pulsed laser technique application to liquid and gaseous flows and the scattering power of seed materials. Appl Optics 24:42-52

Arroyo M, Greated C (1991) Stereoscopic particle image velocimetry. Measurement Science and Technology 2:1181-1186

Barnhart D, Adrian R, Papen G (1994) Phase-conjugate holographic system for high-resolution particle image velocimetry. Applied Optics 33:7159-7170

Bourdon C, Olsen M, Gorby A (2004) Validation of an analytical solution for depth of correlation in microscopic particle image velocimetry. Measurement Science and Technology 15:318-327

Elsinga G, Scarano F, Wieneke B, van Oudheusen B (2006) Tomographic particle image velocimetry. Experiments in Fluids 41:933-947

Forouhar A, Liebling M, Hickerson A, Nasiraei-Moghaddam A, Tsai HJ, Hove J, Fraser S, Dickinson M, Gharib M (2006) The embryonic vertebrate heart tube is a dynamic suction pump. Science 312(5774):751-753

Fouras A, Dusting J, Hourigan K (2007a) A simple calibration technique for stereoscopic particle image velocimetry. Experiments in Fluids 42:799-810

Fouras A, Dusting J, Lewis R, Hourigan K (2007b) Three-dimensional synchrotron x-ray particle image velocimetry. Journal of Applied Physics 102:064,916-064,922

Fouras A, Lo Jacono D, Hourigan K (2008) Target-free Stereo PIV: a novel technique with inherent error estimation and improved accuracy. Experiments in Fluids 44:3170-329

Kahler C (2004) Investigation of spatio-temporal flow structure in the buffer region of a turbulent boundary layer by means of multiplane stereo PIV. Experiments in Fluids 36:114-130

Lo Jacono D, Plouraboué F, Bergeon A (2005) Weak-inertial flow between two rough surfaces. Physics of Fluids 17:63,602-63,612

Meinhart C, Wereley S, Gray M (2000a) Volume illumination for two-dimensional particle image velocimetry. Meas Sci Technol pp 809-814

Meinhart CD, Werely ST, Santiago JS (2000b) A PIV algorithm for estimating time-averaged velocity fields. Journal of Fluids Engineering 122:285-289

Olsen M, Adrian R (2000a) Brownian motion and correlation in particle image velocimetry. Optics and Laser Technology 32:621-627

Olsen M, Adrian R (2000b) Out-of-focus effects on particle image visibility and correlation in microscopic particle image velocimetry. Experiments in Fluids 29:S166-S174

Olsen M, Bourdon C (2003) Out-of-plane motion effects in microscopic particle image velocimetry. Journal of Fluids Engineering 125:895-901

Park J, Kihm K (2006) Three-dimensional micro-PTV using deconvolution microscopy. Experiments in Fluids 40:491-499

Pereira F, Gharib M, Dabiri D, Modarress M (2000) Defocusing DPIV: A 3-component 3-D DPI measurement technique. application to bubbly flows. Experiments in Fluids 29:S78-S84

Schroder A, Kompenhans J (2004) Investigation of a turbulent spot using multi-plane stereo particle image velocimetry. Experiments in Fluids 36:82-90

Willert C, Gharib M (1992) Three-dimensional particle imaging with a single camera. Experiments in Fluids 12:353-358

Zhang J, Tao B, Katz J (1997) Turbulent flow measurement in a square duct with hybrid holographic PIV. Experiments in Fluids 23:373-381